The antibacterial and anti-inflammatory effects of zinc oxide nanoparticles synthesized by *Thymus vulgaris medicinal plant against Escherichia coli and Escherichia coli lipopolysaccharides*

Amal M. Aboelmaaty[a], Shimaa T. Omara[b], Mohamed S. Aly[a], Mohamed S. Kotp[a], Amal H. Ali[a]

Departments of [a]Animal Reproduction and Artificial Insemination, [b]Microbiology and Immunology, Veterinary Research Institute, National Research Centre, Dokki, Egypt

Correspondence to Amal M. Aboelmaaty, PhD, Department of Animal Reproduction and Artificial Insemination, Veterinary Research Institute, National Research Centre, 33 El Buhouth Street, Dokki, Giza, Postal Code 12622, Egypt.
e-mail: amalaboelmaaty1@yahoo.com, am.aly@nrc.sci.eg

Received: 13 December 2021
Revised: 11 January 2022
Accepted: 15 January 2022
Published: 21 July 2022

Egyptian Pharmaceutical Journal 2022, 21:153–166

Background and objectives
The emerging nanotechnology-prepared medications and their applications in industrial and medical fields have gained great progress. This study aimed to investigate the efficacy of zinc oxide nanoparticles (ZnO-NPs) synthesized by the green method using the Thymus vulgaris plant extract against the most common pathogenic bacteria causing endometritis in horses (Escherichia coli) and E. coli lipopolysaccharide (LPS).
Materials and methods
Uterine swabs from mares (n=50) with clinical endometritis were collected for isolating the pathogenic bacteria. A total of 40 Wistar rats were divided equally into control (n=10), LPS (n=10; 10 mg/kg body weight), ZnO-NPs (n=10; 50 mg/kg body weight), and LPS+ZnO-NPs (n=10). ZnO-NPs were administered for 4 days and the LPS on the fourth day. Histopathological and ultrastructures of liver, kidney, and testes were obtained. Blood samples were collected for measuring superoxide dismutase (SOD), malondialdehyde, nitric oxide, and testosterone.
Results and conclusion
ZnO-NPs of 15–30 nm showed antimicrobial effectiveness against the isolated multidrug-resistant *E. coli*. The LD50 for ZnO-NPs was 2000 mg/kg body weight. The histopathological changes showed massive damage to the seminiferous tubules, liver, and kidney of LPS-treated rats, which was reversed to a great extent by preadministration of ZnO-NPs. The activity of SOD was high in LPS and ZnO-NPs, but the LPS+ZnO-NPs and the controls had the lowest SOD activity. LPS and LPS+ZnO-NPs decreased malondialdehyde concentrations. LPS decreased NO, but ZnO-NPs restored control values. Testosterone declined after LPS administration, with no observed changes in the rats treated with ZnO-NPs or LPS+ZnO-NPs. ZnO-NPs proved dual actions of antimicrobial and anti-inflammatory. Short course and suitable dose should be investigated to avoid its cytotoxicity effects to vital organs.

Keywords:
antibacterial, anti-inflammatory, *Escherichia coli*, lipopolysaccharide, rats, zinc nanoparticles

Egypt Pharmaceut J 21:153–166

1687-4315

Introduction

In equine, endometritis is considered a major cause of infertility [1]. Endometritis with mixed bacterial infections involving *Escherichia coli* was highly encountered [2]. Bacterial endometritis is caused by *E. coli* through the binding of its lipopolysaccharide (LPS) with Toll-like receptor 4 of endometrial epithelial cells, which activates mitogen-activated protein kinase and downstreaming nuclear factor κB pathways, stimulating the release of cytokines [2,3]. Both inflammatory mediators and *E. coli* LPS disturb the hypothalamic-pituitary-ovarian axis, suppress ovulation, delay or block the luteinizing hormone surge, reduce estradiol rise, decrease conception, and induce embryonic loss [4]. In rats, a single injection of LPS-induced inflammation, caused a biphasic decline in Leydig cell testosterone production and gonadotropin responsiveness, reduced LH levels, decreased the testicular interstitial fluid formation, but maintained the intra-testicular testosterone concentrations to support qualitatively normal spermatogenesis [5].

The misuse of antibiotics for treatment of bacterial endometritis has led to the generation of bacterial antibiotic resistance [3]. Zinc oxide nanoparticles (ZnO-NPs) could overcome microbial resistance [6]. The antimicrobial activities of ZnO-NPs increased with decreasing their particle size or with increasing

their surface area [7]. In mice, ZnO-NPs in doses of 50 and 500 mg/kg showed minimal toxicity [8], caused kidney and liver toxicity in rats [9], and increased the proinflammatory cytokines in concentration from 0.5 to 20 μg/ml [10]. The daily administration of 2 mg/kg ZnO-NPs for 3 weeks affected the nephron ultrastructure [11].

ZnO-NPs induced cytotoxic effects in the male reproductive system, which eventually compromised male fertility [12], induced apoptosis in Leydig and Sertoli cells with nuclear DNA damage [13,14], and increased the apoptosis of Sertoli and Leydig cells [15].

The present study aimed the following: (a) synthesize and characterize ZnO-NPs by the green method using Thymus plant extracts; (b) to isolate and identify the pathogenic *E. coli* from mares with endometritis; (c) to evaluate antimicrobial resistance profiles of ZnO-NPs *in vitro* using agar well diffusion, minimum inhibitory concentration (MIC), and minimum bactericidal concentration (MBC); (d) to evaluate *in vivo* protective effects of ZnO-NPs against *E. coli* LPS by measuring the blood oxidant, antioxidant status, and testosterone; and (e) to examine the histopathological and ultrastructural changes using transmission electron microscope (TEM).

Materials and methods

Preparation and characterization of zinc oxide nanoparticles

Three types of thymuses (*Thymus bovei*, *Thymus decussate*, and *Thymus origanum*) were used in this study for preparation of ZnO-NPs. For every 1 g of dried Thymus plant, 10 ml of distilled water was added and kept in a shaker incubator at 37°C and 200 rpm for 48 h. The plant extract was then filtered using Whatman filter paper number 1 and kept in the refrigerator at 4°C. For every 10 ml of the plant extract, 1 g of zinc sulfate (molecular weight=287.54; Kock-Light Laboratories Ltd, Colnbrook Bucks, England) was added. The mixture of zinc sulfate and the plant extract is heated on a magnetic stirrer at the highest temperature until complete disappearance of the salt. The shape and the size of the prepared ZnO-NPs were determined using a TEM in the liquid and diluted samples (Fig. 1b). The remaining prepared ZnO-NPs are kept in the shaker incubator at 37°C (200 rpm) until complete evaporation of the liquid, and then the dried powder was characterized using a scanning electron microscope (NRC, QUANTA FEG250) to determine the shape and size of powdered ZnO-NPs (Fig. 1a). Radiograph diffraction was used (Diffractometer system=EMPYREAN, NRC) (42 kV/120 mA) with CuKa radiation, using Ka of the Cu (k=1.542 Å), and the sweep was conducted between 10° and 80°.

Uterine sample collection and isolation, identification, and antibiotic sensitivity of *Escherichia coli*

Uterine swabs/washes (n=50) were taken by sterile guarded swabs/Foley catheters from repeat breeder mares having endometritis and nonresponsive to several antibiotic treatments. Endometritis was confirmed clinically by diagnosis of endometrial fluid, transrectal ultrasonographic examination (SonoAceR3) equipped with a 12-MHz linear-array

Figure 1

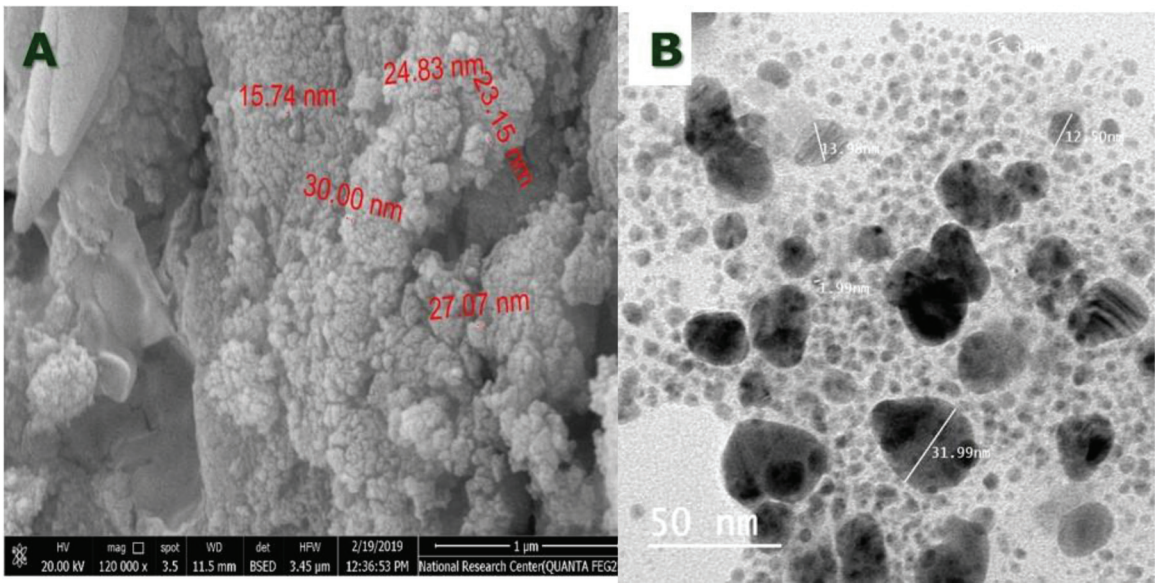

Scanning (a) and transmission (b) electron microscope of ZnO-NPs prepared by thymus extract. ZnO-NP, zinc oxide nanoparticle.

B-mode transducer [16]. The sterile swabs were inoculated into sterile tubes containing recovery broth (Oxoid). The swabs were transferred to the laboratory and analyzed for the presence of *E. coli* by incubating them for 24 h at 37°C. A loopful from each broth was then streaked onto MacConkey's agar (Oxoid, Oxoid Limited, Wade Road, Basingstoke, Hampshire, RG24 8PW, United Kingdom) and then chromogenic agar (Oxoid). All plates were incubated aerobically at 37°C for 24–48 h. Identification of the recovered isolates was done using API kit (Biomerieux) and according to colony appearance, Gram stain analysis, Koneman's Color Atlas, and Textbook of Diagnostic Microbiology [17]. The confirmed isolates were preserved for long term in brain-heart infusion broth (Oxoid) with 15% glycerol at −80°C. Using Mueller-Hinton agar (Oxoid), antimicrobial sensitivity was assessed by the Kirby-Bauer disk diffusion method [18],and then disks were impregnated with cefazolin (KZ 30 μg), amoxicillin/clavulanic acid (AMC 30 μg), gentamicin (Gn 10 μg), cefotaxime (CTX; 30 μg), amikacin (AK; 30 μg), cefepime (FEP 30 μg), cefoxitin (FOX 30 μg), imipenem (IPM 10 μg), ceftazidime (CAZ 30 μg), ciprofloxacin (CIP 5 μg), tetracycline (TE 30 μg), chloramphenicol (C 30 μg), norfloxacin (NOR 10 μg), trimethoprim-sulfamethoxazole (SXT 25 μg), ampicillin (AMP 10 μg), and cephalothin (KF 30 μg). All plates were then incubated at 37°C for 24 h, and the inhibition zones were measured and interpreted [19].

Antibacterial effectiveness, minimum inhibitory concentration, and minimum bactericidal concentration of the autoclaved and nonautoclaved zinc oxide nanoparticles

A stock solution of powdered ZnO-NPs (333.3 mg/ml saline) was prepared. Half of the ZnO-NP stock solution was autoclaved at 121°C for 20 min. Then, different dilutions of autoclaved and nonautoclaved ZnO-NPs were tested for their antimicrobial effectiveness against clinically isolated *E. coli*. Another four dilutions were made from the stock solution (first stock=0.333 mg/μl, second 75%= 0.250 mg/μl, third 50%=0.167 mg/μl, fourth 25%= 0.083 mg/μl, and fifth 10%=0.033 mg/μl). All dilutions were tested through agar well diffusion method. Mueller-Hinton agar plates were prepared with a uniform thickness of ~4 mm, then allowed to set at ambient temperature to solidify, and then wells were formed in each agar plate. A swab spreading of 0.5 McFarland concentrations of overnight cultured *E. coli* was done onto the surface of Mueller-Hinton agar medium. Then, 100 μl of ZnO-NP dilutions was added into the formed agar wells of Mueller-Hinton agar. The plates were then left at room temperature for 30 min to allow the diffusion of ZnO-NPs. Then, the plates were incubated at 37°C for 24 h. The antimicrobial effectiveness was calculated by measuring the diameters of the inhibition zones. The MIC and MBC were determined for the autoclaved ZnO-NP dilutions using six sterile 13×100 mm tubes closed with metal caps. From the prepared and autoclaved stock solution of dried ZnO-NPs (333.3 mg/ml saline), two-fold serial dilutions were done using Mueller-Hinton agar broth to prepare various concentrations (166.7, 83.3, 41.7, 20.8, 10.4, and 5.2 mg/ml) using the broth macro-dilution method by adding 1 ml of serially diluted ZnO-NPs to 1 ml of the adjusted bacterial concentration inoculums (5×10^5 CFU/ml). The test tubes were then incubated at 37°C for 18–20 h. The lowest concentration of ZnO-NPs that inhibited the bacterial growth was considered as the MIC [19]. Aliquots of 100 μl from each test tube that did not show any bacterial growth were streaked onto BHI agar (Oxoid) plates and then incubated at 37°C for 20 h. The lowest concentration of ZnO-NPs that killed 100% of the initial bacterial population on the BHI agar was considered the MBC [19].

Determination of LD50 of zinc oxide nanoparticles

Before performing any laboratory animal experiments, the Animal Care and use Committee approval (National Research Centre Medical Research Ethics Committee number (19–143) was obtained. Albino mice (n=42) of either sex, weighing between 25 and 30 g, belonging to the NRC animal laboratory were distributed equally into seven groups and administered orally 100, 200, 400, 600, 800, 1000, and 2000 mg/kg body weight. LD50 of ZnO-NPs is calculated by determining the dose that causes 50% mortality of the mice within 24–48 h. After administration, the skin and fur changes, eye secretion, and respiration and behavior patterns of the mice were observed. Special attention was paid to the signs of toxicity including tremors, convulsions, salivation, nausea, vomiting, diarrhea, lethargy, and coma [20].

Animals

Male Wistar albino rats (body weight: 150–200 g) were purchased from the animal house of Faculty of Medicine, Cairo University, and kept there until the end of the experiment. Rats (n=40) were equally divided into four groups. The control group received an intraperitoneal (i.p.) injection of physiological saline (0.9% NaCl) for four successive days. The LPS group received saline i.p. for three successive days and then 10 mg/kg LPS (LPS of *E. coli* O111:B4; Sigma, St

Louis, Missouri, USA) dissolved in saline on day 4. The ZnO-NPs group was administered i.p. 50 mg/kg body weight ZnO-NPs dissolved in distilled water for four successive days [21]. The LPS+ZnO-NPs group received 50 mg/kg body weight ZnO-NPs i.p. for four successive days and LPS (10 mg/kg) on day 4. One day after the last dosing (day 5), all animals were anesthetized with chloroform and killed.

Blood and tissue sampling, oxidants, antioxidants, and testosterone measurements

Blood samples were collected in blank vacuum tubes, centrifuged for 10 min at 3000 rpm to separate the serum, and then the animals were killed after anesthesia. The testicles, liver, and kidneys were harvested for histopathological examinations. On the contrary, liver and kidney of animals treated with ZnO-NPs and LPS+ZnO-NPs were preserved in 4% glutaraldehyde buffer for electron microscope examinations. Measurements of superoxide dismutase (SOD), nitric oxide (NO), and lipid peroxide product [malondialdehyde (MDA)] were done in blood sera using commercial diagnostic kits (Biodiagnostic, Cairo, Egypt). Testosterone was assayed using quantitative enzyme immunoassay (Catalog Number: BC-1115 MYM Laboratory and Medical Supply Inc., San Diego, California, USA). The sensitivity of the assay was 0.05 ng/ml, and intra-assay and interassay precisions were 10 and 8.4%, respectively.

Histopathological examinations and ultrascanning with the transmission electron microscope

For histopathological examination, the excised testes, liver, and kidney were washed with physiological saline, sliced into small pieces (2–3 mm^3), and fixed in 10% neutral buffered formalin. After dehydration and clearing in xylene, tissues were embedded in paraffin; 4–6-μm sections were cut and stained with hematoxylin and eosin. The sections were viewed and photographed with the camera of Olympus light microscope (Olympus BX51, Tokyo, Japan) [22].

For electron microscopic examination, sections of 1 mm^3 of liver and kidney were preserved in a 4% glutaraldehyde solution (pH 7.3). Samples were fixed from outside using glutaraldehyde buffer (pH 7.3) for 2 h. For the inner fixation of the sample, osmium tetroxide (0.1 M) was used for 2 h. The sample was then dehydrated through ethanol series (30, 50, 70, 90, and 100%); the time of dehydration in each concentration was 10 min except for the last one, which needed 30 min. After fixation with buffered fixatives and the dehydration using increasing concentrations of ethyl alcohol, dehydration continued by increasing concentration of a solvent (a combination of ethyl alcohol 50% with propylene oxide 50%) for 10 min and propylene oxide 100% for 10 min to enable infiltration with a liquid resin. Samples were passed through a transition solvent (propylene oxide 50% and resin 50%) for 1 hand embedded in a liquid resin (100%) for 1 h. After embedding the samples in the resin block and keeping for 24 h at 60°C, an ultra-microtome was used to slice the samples into semithin sections (50–70 nm thickness), which were collected on metal mesh 'grids' and stained with Toluidine blue for light microscopy orientation and selecting of a small area for ultra-thin sectioning. Ultrathin sections of 50–70 nm were made using a diamond knife and were placed/collected on a grid of metal.

Statistical methods

Data were analyzed using IBM SPSS software (2016, version 20.0) and expressed as mean±SEM. One-way analysis f variance was applied to test the significance of biochemical data of different groups followed by Duncan's multiple range test. Results were considered significant when P value less than or equal to 0.05.

Results

The morphology of the synthesized ZnO-NPs shows aggregation, with a mean size of 23.71 nm and ranged from 15.74 to 30 nm (Fig. 1a). With the TEM, ZnO-NPs had the shape of polygonal spheres, and their diameters ranged from 5.3 to 31.99 nm (Fig. 1b).

Of 50 examined uterine swabs of repeat breeder mares, 11 indicated *E. coli* (22%). The *E. coli* recovered from mares with endometritis showed a broad and variable antimicrobial resistance profile with complete resistance (100%) against amoxicillin/clavulanic acid, ampicillin, ciprofloxacin, tetracycline, gentamicin, and trimethoprim-sulfamethoxazole, followed by amikacin (91%), cephalothin 72.7%, cefotaxime 63.6%, ceftazidime 54.6%, and cefazolin 45.5%, and was 36.4% against each of cefoxitin, cefepime, imipenem, and chloramphenicol (Table 1; Fig. 2a, b). Compared with the nonautoclaved ZnO-NPs (Fig. 2d), the autoclaved ZnO-NPs (Fig. 2c) showed higher antimicrobial effectiveness against the isolated *E. coli* at a concentration of 0.333 mg/μl (Fig. 3) and showed the maximal MIC and MBC of 20.8 (Fig. 2e) and 166.7 mg/ml, respectively (Fig. 2f).

The LD50 of ZnO-NPs was 2000 mg/kg body weight. Other doses less than 1000 mg/kg body weight did not

Table 1 Resistance profiles of *Escherichia coli* recovered from mares with endometritis

Antimicrobial		Resistance phenotype of *Escherichia coli* (*N*=11 isolates)
Name	Concentration	*n* (%)
Amoxicillin/clavulanic acid (AMC)	30 μg	11 (100)
Ampicillin (AMP)	10 μg	11 (100)
Ciprofloxacin (CIP)	5 μg	11 (100)
Tetracycline (TE)	30 μg	11 (100)
Gentamicin (CN)	10 μg	11 (100)
Amikacin (AK)	30 μg	10 (91)
Trimethoprim-sulfamethoxazole (SXT)	25 μg	11 (100)
Norfloxacin (NOR)	10 μg	3 (27.3)
Cephalothin (KF)	30 μg	8 (72.7)
Cefazolin (KZ)	30 μg	5 (45.5)
Cefoxitin (FOX)	30 μg	4 (36.4)
Cefotaxime (CTX)	30 μg	7 (63.6)
Ceftazidime (CAZ)	30 μg	6 (54.6)
Cefepime (FEP)	30 μg	4 (36.4)
Imipenem (IPM)	10 μg	4 (36.4)
Chloramphenicol (C)	30 μg	4 (36.4)

kill any animal and showed neither toxicity signs nor abnormal behaviors.

The testicles of control groups showed normal histological architecture, multiple seminiferous tubules lined with several rows of spermatogonial cells, interstitial cells in between, and normal spermatogenesis with normal sperm production (Fig. 4a). The ZnO-NPs group showed normal structures with mild intertubular edema (Fig. 4b). The LPS group (Fig. 4c) showed severe disruptive effects and pathological alterations, severe atrophy of seminiferous tubules, severe interstitial edema, and congested blood vessels. The LPS group showed degenerated spermatogonial cells and Sertoli cells, primary and secondary spermatocytes, spermatids, and Leydig cells with loss of sperm cell population. The testicles of LPS+ZnO-NPs group appeared normal with mild intertubular edema and amelioration of these histopathological changes (Fig. 4d). The hepatic tissue of the control rats showed a normal histological architecture of the hepatic lobule (Fig. 5a). ZnO-NPs showed normal liver structure with mild congestion of central veins and mild spacing of blood sinusoids (Fig. 5b). LPS (Fig. 5c) exhibited severe histopathological changes, which were characterized by dilation of the blood sinusoids, multifocal leukocytic cell infiltration associated with severe hemorrhage and congestion of hepatic blood sinusoids, and vacuolar degeneration and necrosis of the hepatocytes. The administration of LPS +ZnO-NPs resulted in the attenuation of these pathological lesions with mild dilation of the blood sinusoids, mild vacuolar degeneration, and mild vascular congestion (Fig. 5d). The kidney of control rats showed normal renal structure (Fig. 6a); ZnO-NPs showed normal renal structure with mild congestion and mid leukocytic cells infiltration (Fig. 6b); LPS induced significant histopathological degenerative changes, including degeneration of tubular cells lining renal tubules, glomerular tuft atrophy, severe hemorrhage, and leukocytic cell infiltration (Fig. 6c); and LPS+ZnO-NPs reduced renal degeneration, vascular congestion, and glomerular atrophy with the presence of mild congestion of renal blood vessels (Fig. 6a).

The ultrastructure (TEM) of rats' kidney treated with ZnO-NPs showed normal glomerular capillary, several elongated mitochondria, black zinc particles, intact glomerular capillary basement membrane with red blood cell, peroxisome with a circular outline, and homogeneous contents are present in the basal region of the cell endoplasmic reticulum (Fig. 7a–c). The nucleus with an intact nuclear membrane, endosomes, lysosomes, cytoplasm, and peroxisomes showed characteristic angular outlines. The TEM of the kidney for rats treated with both LPS+ZnO-NPs showed cells with fewer organelles (mitochondria, nucleus, nucleolus, endosomes, lysosome, and zinc particles) with cell evacuated from its organelles except the nucleus (Fig. 7e,f).

The liver TEM of rats treated with ZnO-NPs (Fig. 8a–d) demonstrated multiple mitochondria, glycogen granules, and endoplasmic reticulum, but those administered LPS showed evacuated cells from the organelles, caused dominance of the endoplasmic

Figure 2

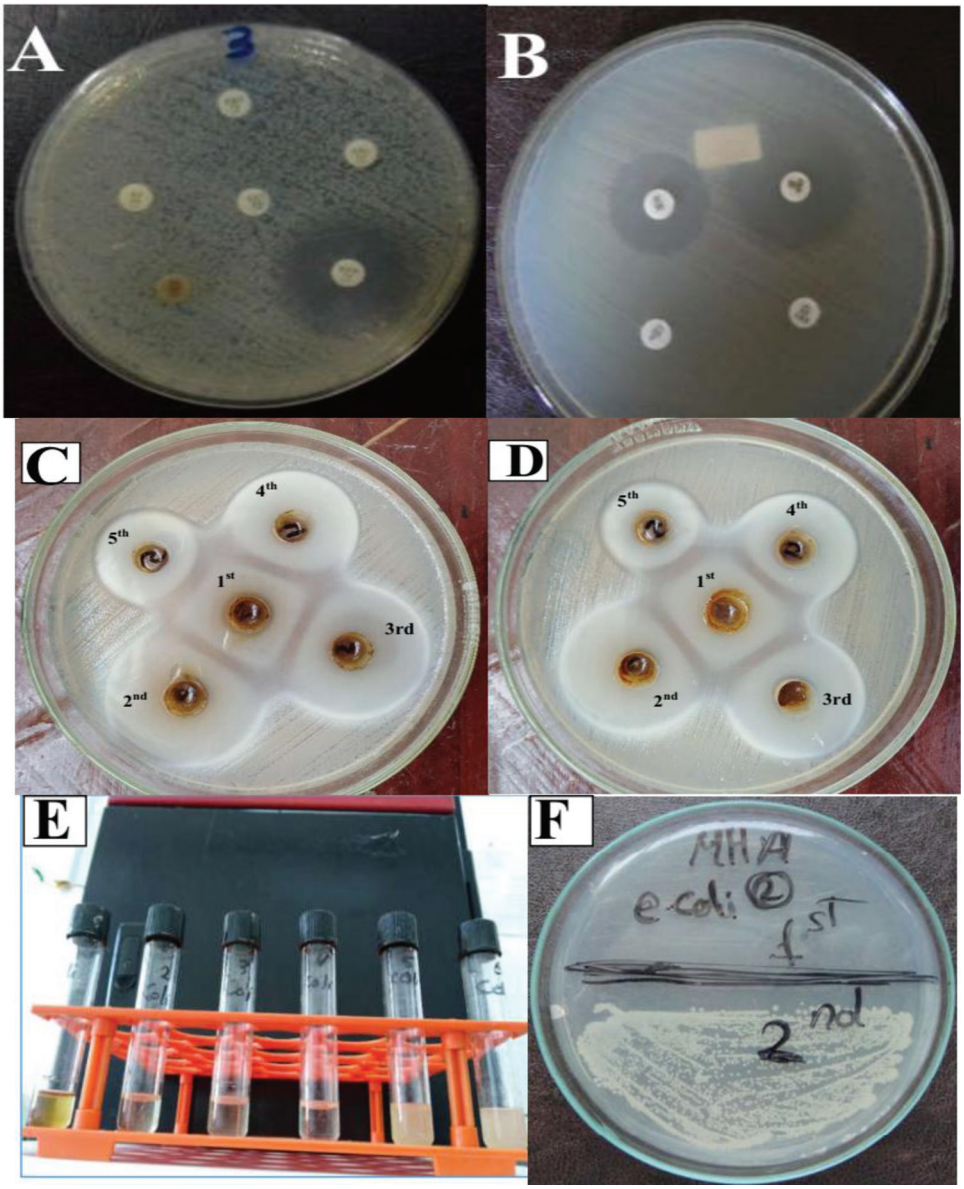

Antimicrobial susceptibility patterns of *Escherichia coli* to antimicrobial disks on Mueller-Hinton agar plate (a, b). Antimicrobial effectiveness of the prepared autoclaved (c) and nonautoclaved (d) ZnO-NP dilutions against *E. coli* using the agar well diffusion method and Mueller-Hinton agar plate. First stock=0.333 mg/µl, second 75%=0.25 mg/µl, third 50%=0.1666 mg/µl, fourth 25%=0.0833 mg/µl, and fifth 10%=0.0333 mg/µl. The MICs (e) and MBC (f) of ZnO-NPs against clinically isolated *E. coli*. MBC, minimum bactericidal concentration; MIC, minimum inhibitory concentration; ZnO-NP, zinc oxide nanoparticle.

reticulum, more lipids, few and hardly demarcated mitochondria, and the nucleus contained less chromatin (Fig. 8e–h).

The LPS and LPS+ZnO-NPs decreased ($P<0.0001$) MDA, but LPS+ZnO-NPs increased ($P<0.0001$) SOD activity. Meanwhile, LPS decreased NO levels ($P<0.0001$) and testosterone ($P<0.002$) concentrations (Table 2).

Discussion

E. coli is one of the major causes of chronic equine endometritis [23]. A higher percentage (39.8%) of multidrug-resistant *E. coli* was isolated from infertile mares [24]. *E. coli* isolates in this study indicated a broad antimicrobial resistance pattern against most penicillins, tetracyclines, ciprofloxacin, trimethoprim, and chloramphenicol [24].

In the current study, ZnO-NPs showed tremendous antibacterial efficiency, and the inhibition zone ranged from 26 to 45 mm for all concentrations (Fig. 3). In a previous study, when SEM and TEM were performed for the bacterial cells treated with ZnO-NPs, both indicated cell membrane disintegration, accumulation of ZnO-NPs in the cytoplasm, and interaction with

Figure 3

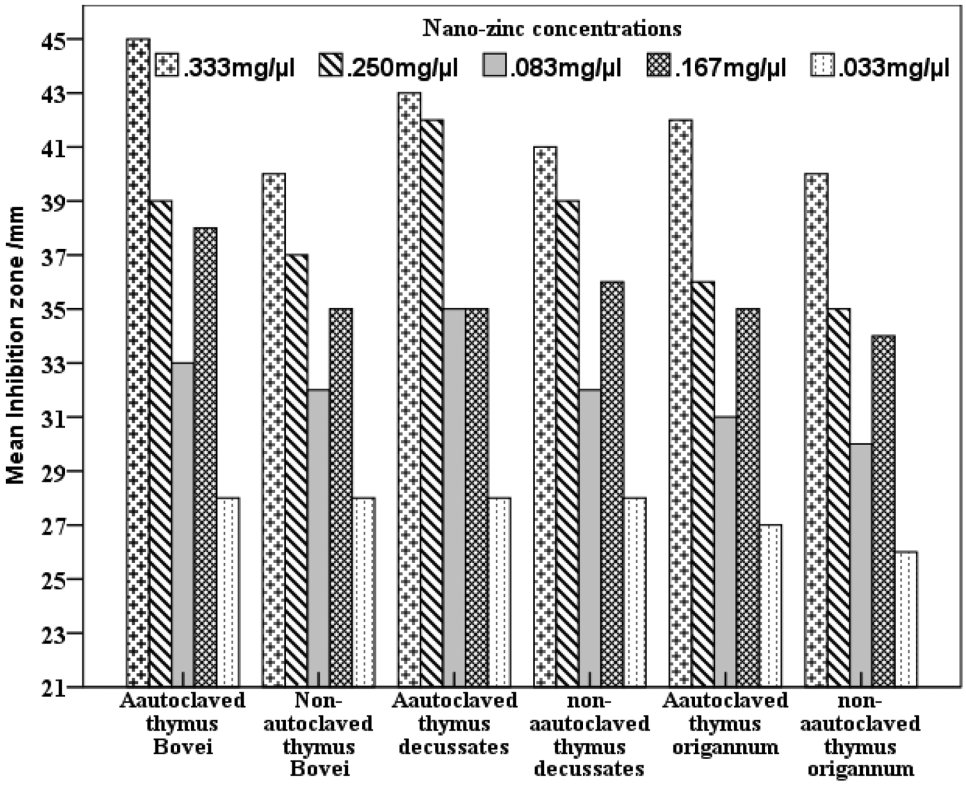

Antimicrobial effectiveness of different concentrations of autoclaved (a) and nonautoclaved (N) ZnO-NPs against *Escherichia coli* (mm) using the agar well diffusion method. ZnO-NP, zinc oxide nanoparticle.

biomolecules causing cell apoptosis and bacterial cell death [25]. The autoclaved ZnO-NPs showed higher antimicrobial effectiveness than the nonautoclaved, with the widest zone of inhibition (45 mm) observed in case of autoclaved ZnO-NPs prepared by *T. bovei* aqueous plant extract. Similarly, ZnO-NPs inhibited the growth of *E. coli* at different concentrations (20–60 µg/ml) using the agar disk diffusion method [26]. ZnO-NPs at a concentration of 0.72 mg/ml produced 10-mm zone of inhibition [27], 100 µg/ml exhibited 17-mm zone of inhibition [28], and 0.4 mg/ml increased the zone of inhibition to 23±0.5 mm [29], indicating better antibacterial activity with lower concentrations. On the contrary, various concentrations of ZnO-NPs showed inability to inhibit *E. coli* [30]. The autoclaved ZnO-NPs prepared by *T. bovei* showed the lowest MIC (20.8 mg/ml) and MBC (166.7 mg/ml). The MIC of green route-prepared ZnO-NPs was 5 µg/ml [26], 40 mg/l [31], and 156.2 µg/ml [32]. These differences depend on the original source of the zinc and the plant used for preparation of the nanoparticles.

ZnO-NPs have shown to be safe nontoxic antimicrobial agents besides being well biocompatibility with human and animal cells when used at an appropriate concentration [27]. ZnO-NPs have the ability to reserve the antioxidant enzymes to inhibit the capability of removing ROS [33]. The formation of active free radicals on the surface of the ZnO-NPs eradicated the bacteria through disrupting the bacterial cell components [34]. Antimicrobial activity of ZnO-NPs depends on the sensitivity of microorganisms, the particle size and morphology, pH, and the concentration [35].

LPS in *E. coli* is one of its cell wall components that is responsible for endometritis. It is known that endometrial cells prompt Toll-like receptor 4 for identification of the LPS endotoxin of gram-negative bacteria leading to interleukins secretion (IL-6 and IL-8) [36]. The anti-inflammatory effects of ZnO-NPs in rats treated with LPS of *E. coli* were evident by histopathology and TEM of testis, liver, and kidney, which were associated with mild cytotoxicity that did not influence neither testosterone nor the oxidative stress parameters. On the contrary, ZnO-NPs induced mechanical harm to *Saccharomyces cerevisiae*, which changed the cell morphology, distorted the membranes, led to spillage of intracellular structures [37], distorted mitochondria [38], and led to the outflow of specific organelles

Figure 4

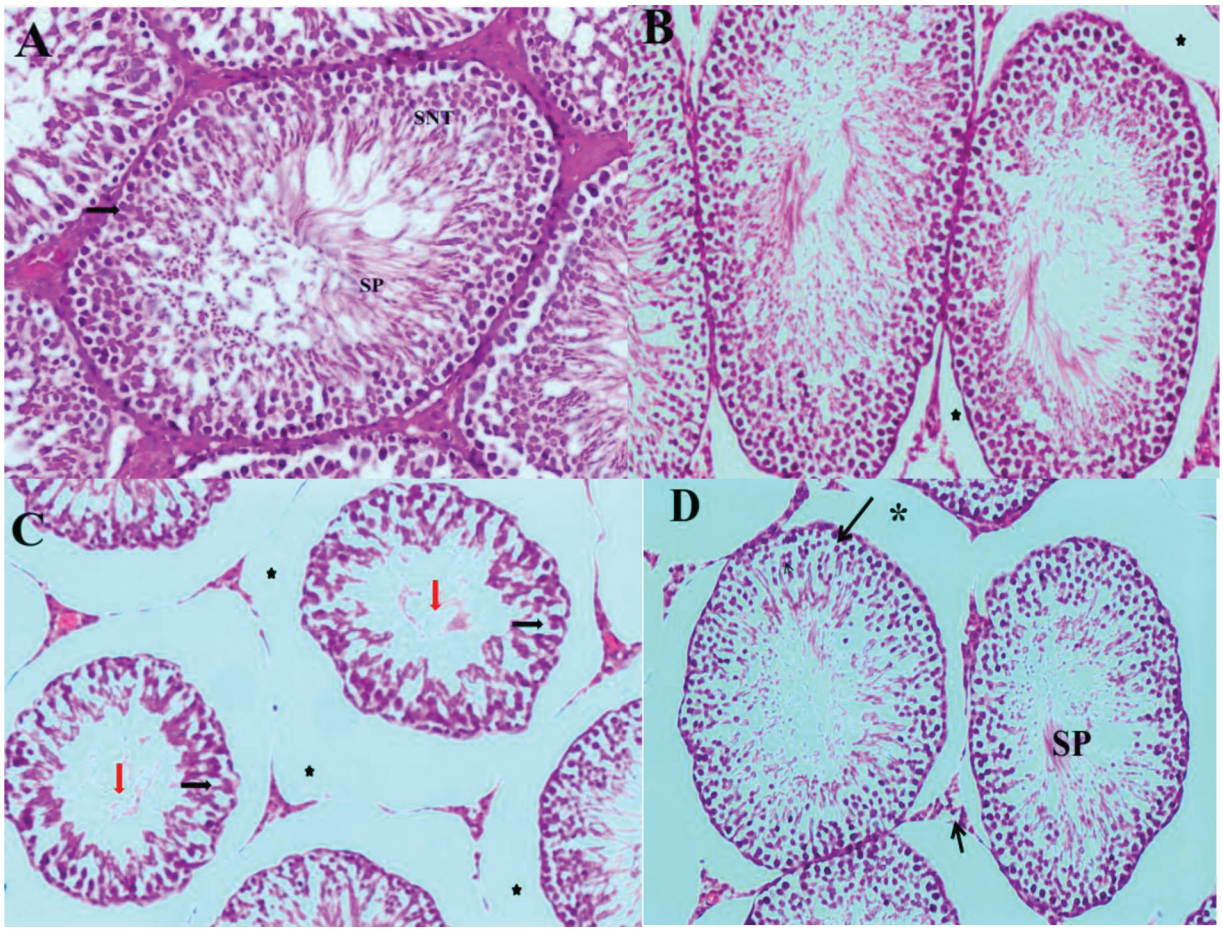

Hematoxylin and eosin (×10) of testicular section of the control rat (a) showing normal seminiferous tubules (SNF) lined with several rows of spermatogonial cells (arrows), with interstitial cells in between, and normal spermatogenesis with intraluminal sperm production (SP). Zinc nanoparticles-treated rats (b) show mild interstitial edema (*). LPS-treated rats (c) show severe atrophy of seminiferous tubules, severe interstitial edema (*), and degenerated spermatogonial cells (black arrow), Sertoli's cells, primary and secondary spermatocytes, spermatids, and Leydig cells, associated with congested blood vessels and loss of sperm cell population (red arrows). Co-LPS+zinc nanoparticles (d) ameliorated these histopathological changes but with mild interstitial edema (*). LPS, lipopolysaccharide.

[39]. These effects were not evident in rats' liver and kidney of our experiment when LPS+ZnO-NPs were administered. This could be attributed to the selective ability of Zn-NPs in enhancing cytotoxicity, destructing the pathogens, and acting as an anticancer agent [40].

In agreement with our observation using TEM, the presence of Zn-NPs intracellularly in the liver and kidney cells could be referred to their ability to build penetrability by obliterating lipid and proteins of the cell membrane and puncturing the cell separator materials to empower them [41]. Similarly, our previous study used the same dose of LPSs of *E. coli* with three other protectors and revealed that the normal euchromatic nucleus and mitochondria in the renal tissue of nontreated control rats were different when compared with the swollen mitochondria, many vacuoles, and residual bodies in rats treated with LPS. Similarly, in animals treated with ZnO-NPs and then LPS, mitochondria were few and swollen with many vacuoles [42].

The increased SOD activity in rats treated with ZnO-NPs in this study could be attributed to reversing of the mild distorting effects of ZnO-NPs on testes, liver, and kidney. Moreover, SOD activity and mRNA expression increased in diabetic rats treated with ZnO-NPs owing to decreased lipid peroxidation of the testicular tissue induced by diabetes, which is similar to their protection against LPS toxic effects [43]. In contrast, doses higher than 600 mg/kg body weight of ZnO-NPs reduced SOD and increased MDA [44]. Similar to kidney and liver ultrastructures treated with either ZnO-NPs or LPS +ZnO-NPs, *in vitro* Leydig cells treated with ZnO-NPs showed autophagosomes, autolysosomes, and autophagic vacuoles [45]. These cytotoxic effects of ZnO-NPs on Leydig cells *in vitro* were not observed in the current study by administering ZnO-NPs *in vivo*.

Figure 5

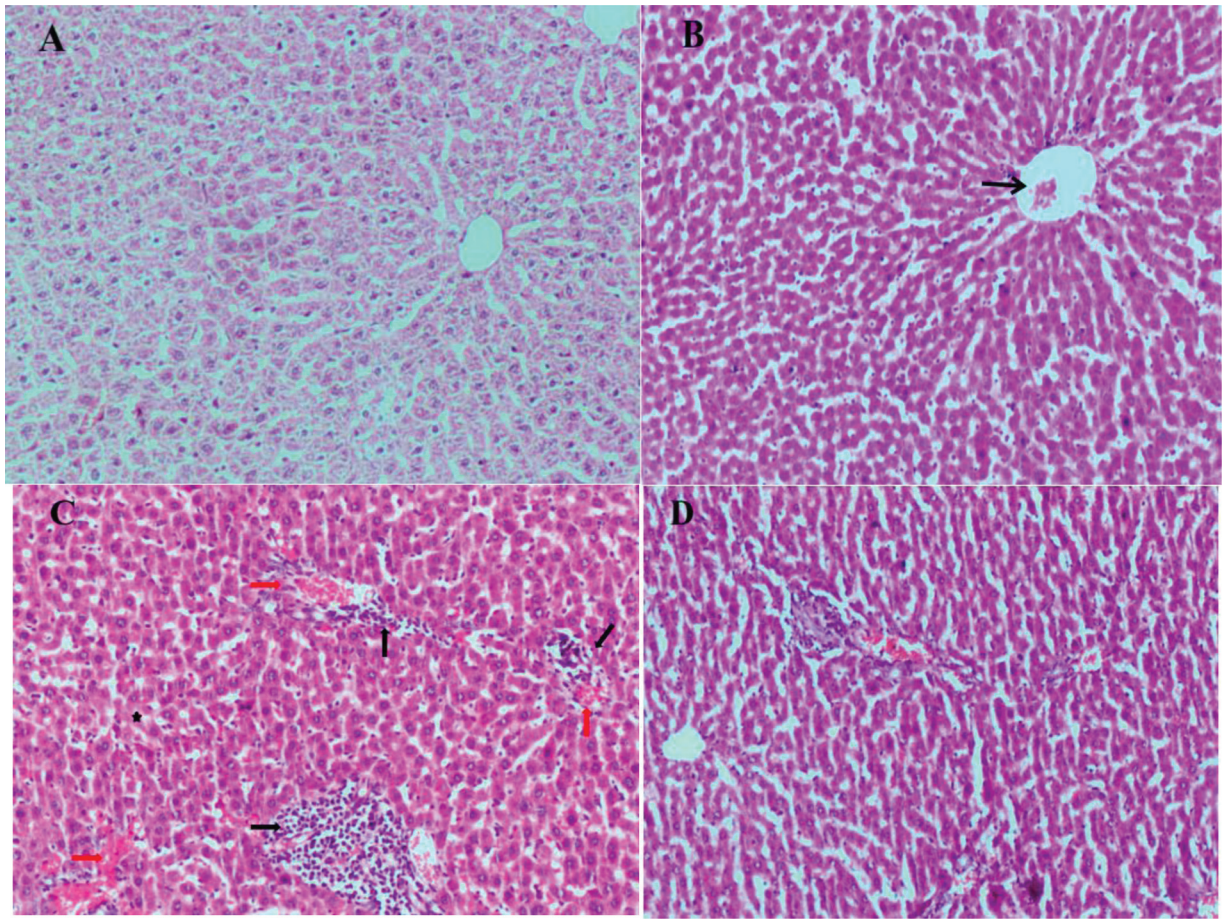

Hematoxylin and eosin (×10) liver of the control rat (a) shows the normal histological architecture of the hepatic lobule, hepatocytes, and sinusoid hepatocytes and sinusoids. Zinc nanoparticles-treated rats (b) show normal liver structure with mild congestion of central veins and mild spacing of blood sinusoids. LPS-treated rats (c) show dilated blood sinusoids, multifocal leukocytic cell infiltration (black arrow) associated with severe hemorrhage (red arrow) and congestion of hepatic blood sinusoids. The hepatocytes show vacuolar degeneration and necrosis (*). LPS-zinc nanoparticles-treated rats (d) show mild dilation of the blood sinusoids, mild vacuolar degeneration, and mild vascular congestion. LPS, lipopolysaccharide.

The increased testosterone in rats treated with ZnO-NPs or LPS+ZnO-NPs was attributed to the increased expression of steroidogenesis-related genes and decreased SOD gene expression [45]. The incubation of Leydig cells *in vitro* with ZnO-NPs for 4 h increased testosterone production 12 h later [15]. Similar to the testicular abnormalities recorded in rats treated with LPS, rats treated with nicotine alone or with ZnO-NPs demonstrated mild to severe testicular structural changes together with sperm morphological abnormalities in the nicotine-treated rats [15].

The improvement induced by administering Zn-NPs before and with the LPS on testicular tissue was also noticed when diabetic rats were treated with 10 mg/kg body weight. ZnO-NPs with and without insulin by increasing the sperm count and motility [43]. The dose of ZnO-NPs injected in rats of the current experiment was not toxic because the toxic effect of ZnO-NPs significantly decreased the sperm cell count, sperm motility, live and normal sperms, serum testosterone level, and antioxidant enzymes activity and causes severe histopathological damage with increased lipid peroxidation [46]. The decrease of testosterone and severe testicular damage in rats treated with LPS in this study were attributed to the severe inflammation that inhibited Leydig cell function and compromised spermatogenesis *in vitro* with increasing LPS concentration [5]. These pathological changes of the spermatogenic function during severe inflammation were directly induced by the effect of inflammatory mediators on the seminiferous epithelium or testicular vasculature [47]. In agreement with our results, the bacterial LPS inhibited testicular steroidogenesis and disrupted the spermatogenesis [47]. In rats, the proinflammatory cytokines and the oxidative stress resulting from LPS affected spermatogenic and steroidogenic functions while disrupting the germ cell layer in testicular seminiferous tubules [48]. The

Figure 6

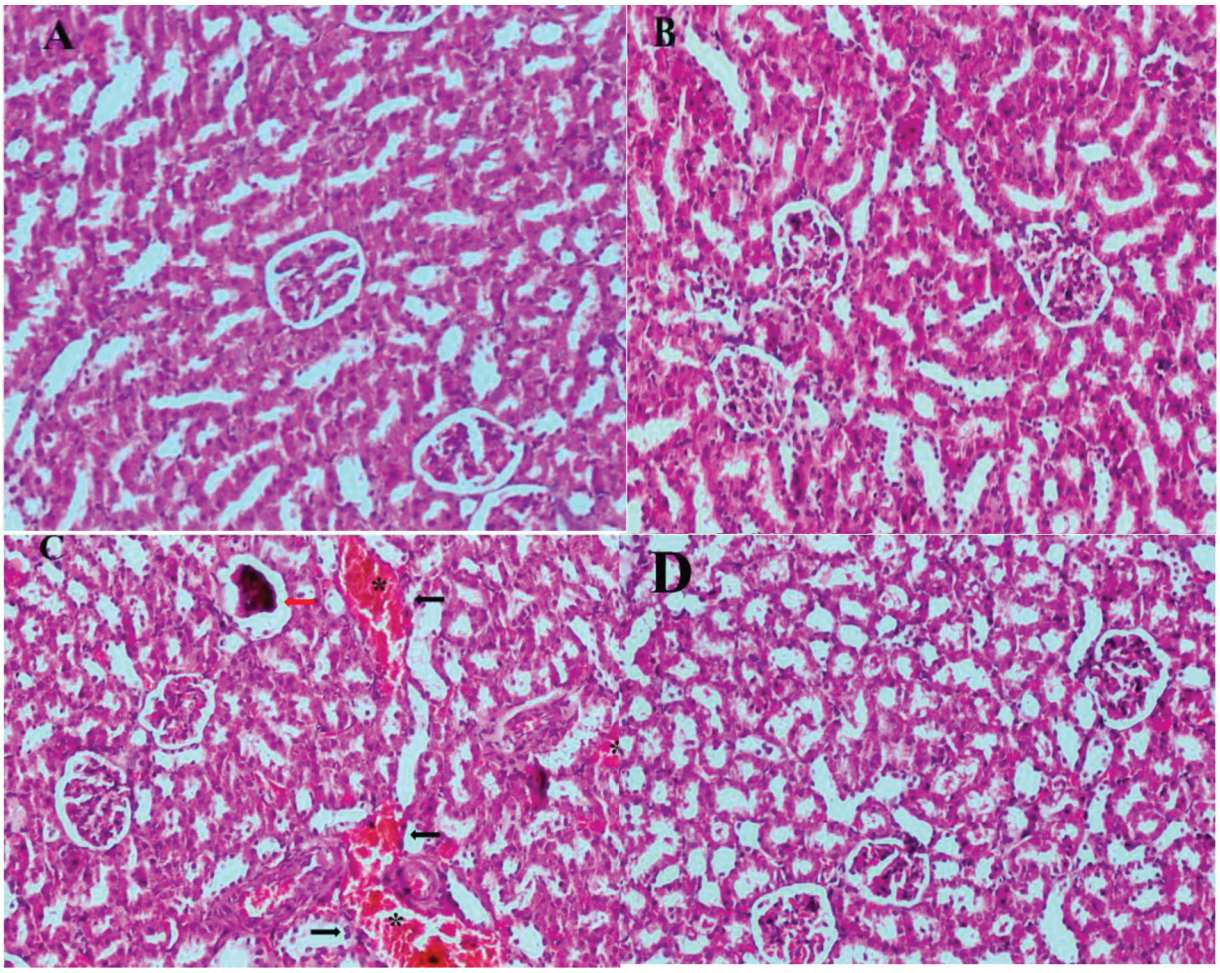

Hematoxylin and eosin (×10) kidney of control rats (a) shows normal renal histologic structure. Zinc nanoparticles-treated rats (b) show normal renal structure with mild congestion and mild leukocytic cell infiltration. LPS-treated rats (c) show degeneration of tubular cell lining of renal tubules, glomerular tuft atrophy (black arrow), severe hemorrhage (*), and leukocytic cell infiltration (red arrow). Zinc nanoparticle and LPS-treated rats (d) reduced the renal degeneration, vascular congestion, and glomerular atrophy and showed mild congestion of renal blood vessels. LPS, lipopolysaccharide.

histopathological alterations associated with LPS administration included severe atrophy of seminiferous tubules, severe interstitial edema, congested blood vessels, necrosis and degenerative changes of the lining of epithelium of seminiferous tubules, and loss of sperm cell population, in line with the impairment of testicular function owing to lipid peroxidation, oxidative stress, reduced testicular antioxidant capacity, and the direct effect of inflammatory mediators on the seminiferous lining epithelium [49–51]. Currently, the protective effect of ZnO-NPs against LPS adverse effects was better than the use of Intermedin to attenuate the LPS-induced testicular inflammation in rats [52]. Concerning liver histopathology and TEM, LPS induced harmful effects to the point of cell damage [49]. Liver of the rats exposed to LPS in this study exhibited severe histopathological changes: multifocal leukocytic cells infiltration, severe hemorrhage, vacuolar degeneration, and necrosis of hepatocytes [52]. LPS treatment increased DNA damage and apoptosis, induced oxidative stress in hepatic cells, and resulted in cell damage [53–55]. Kidney of LPS-treated rats showed significant degenerative changes, including degeneration of tubular cells lining renal tubules, glomerular tuft atrophy, severe hemorrhage, and leukocytic cell infiltration [52,56].

In the kidney, the longer (3 weeks) the treatment with lower doses of ZnO-NPs (2 mg/kg body weight of 35 nm size), the more alterations of the glomeruli accompanied with vascular alterations in the capillaries of the glomeruli, podocytes hypertrophy and degenerative changes, basement membrane thickening, granulation and shrinkage of nuclei together with reduction in the number and widening of podocyte pedicels, and lysosomal accumulation, and the basolateral plasma membrane enfolding of the renal

Figure 7

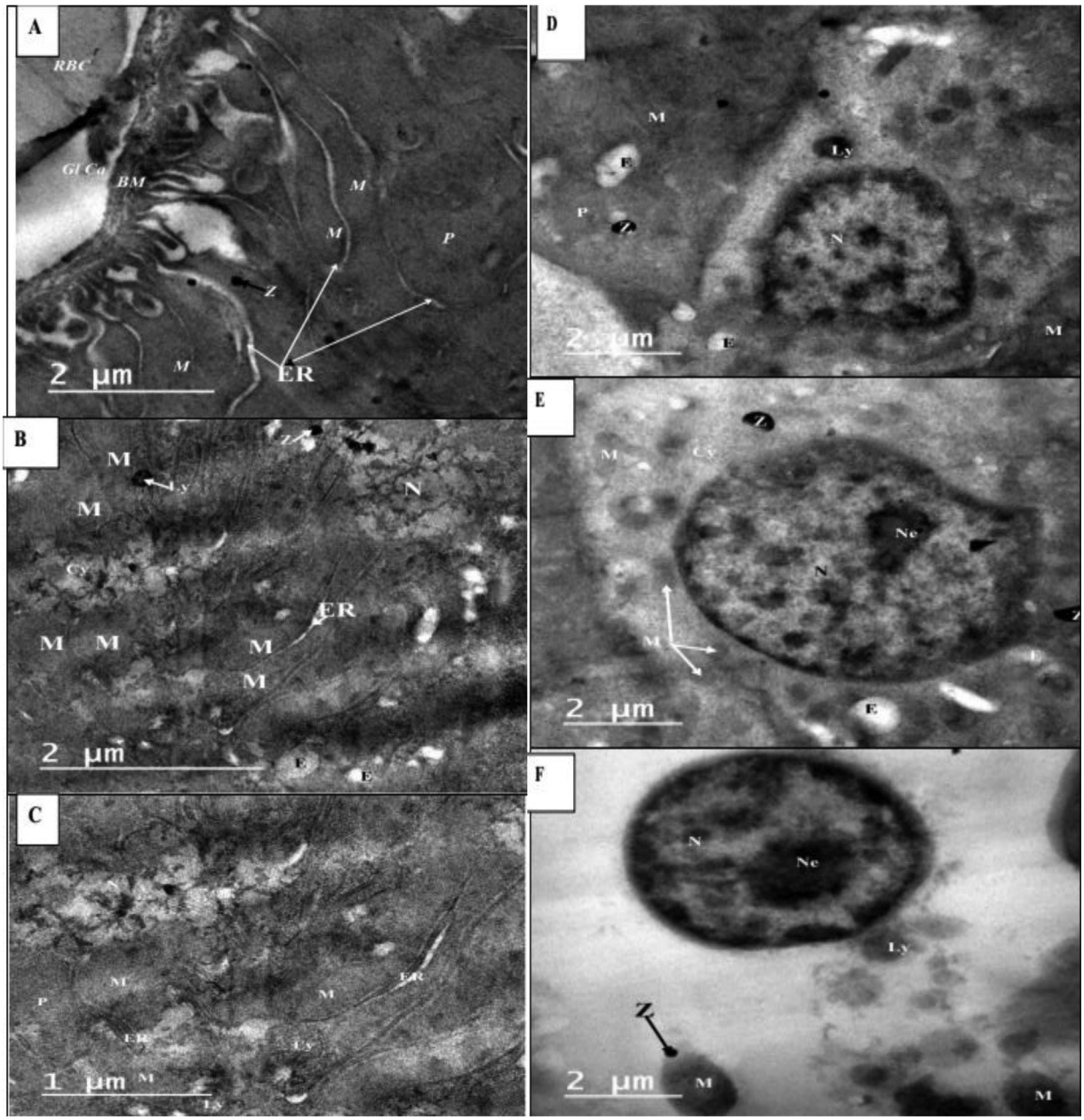

TEM of the rat's kidney treated with zinc nanoparticles shows the glomerular capillary (Gl Ca), elongated mitochondria (M) zinc particles (Z, black arrow), basement membrane (BM), red blood cell (RBC), peroxisome (P), with a circular outline and homogeneous contents being present in the basal region of the cell endoplasmic reticulum (white arrows, a); nucleus (N), endosomes (E), lysosomes (Ly), cytoplasm (Cy, b); Peroxisomes (p) with characteristic angular outlines (c). TEM of the kidney in rats treated with zinc nanoparticles and the LPS (d–f) showing the nucleus (N), nucleolus (Ne), few mitochondria (M), lysosomes (Ly), endosomes (E), and zinc particles (Z). LPS, lipopolysaccharide; TEM, transmission electron microscope.

cells of this group of rats was not as deep as seen in the control [11]. In rats, LPS induced degeneration of tubular cell lining of renal tubules, glomerular tuft atrophy, severe hemorrhage, and leukocytic cell infiltration in the kidney [54,56]. The administration of doses of ZnO-NPs with 10–30 nanometer size (4, 8, 25, 50, 100, and 200 mg/kg) twice a week for 4 weeks in female rats increased the inflammatory cell infiltration and induced fibrosis at high concentrations [57].

Conclusion

The autoclaved eco-friendly green route-synthesized ZnO-NPs prepared using Thymus plant extracts showed excellent antimicrobial effects against clinically isolated multidrug-resistant *E. coli* from mares with endometritis. The green route-synthesized ZnO-NPs ameliorated the inflammatory effects produced by the LPS of the *E. coli*. Further studies are needed regarding application of nano-medicine formulations of ZnO-NPs in the

Figure 8

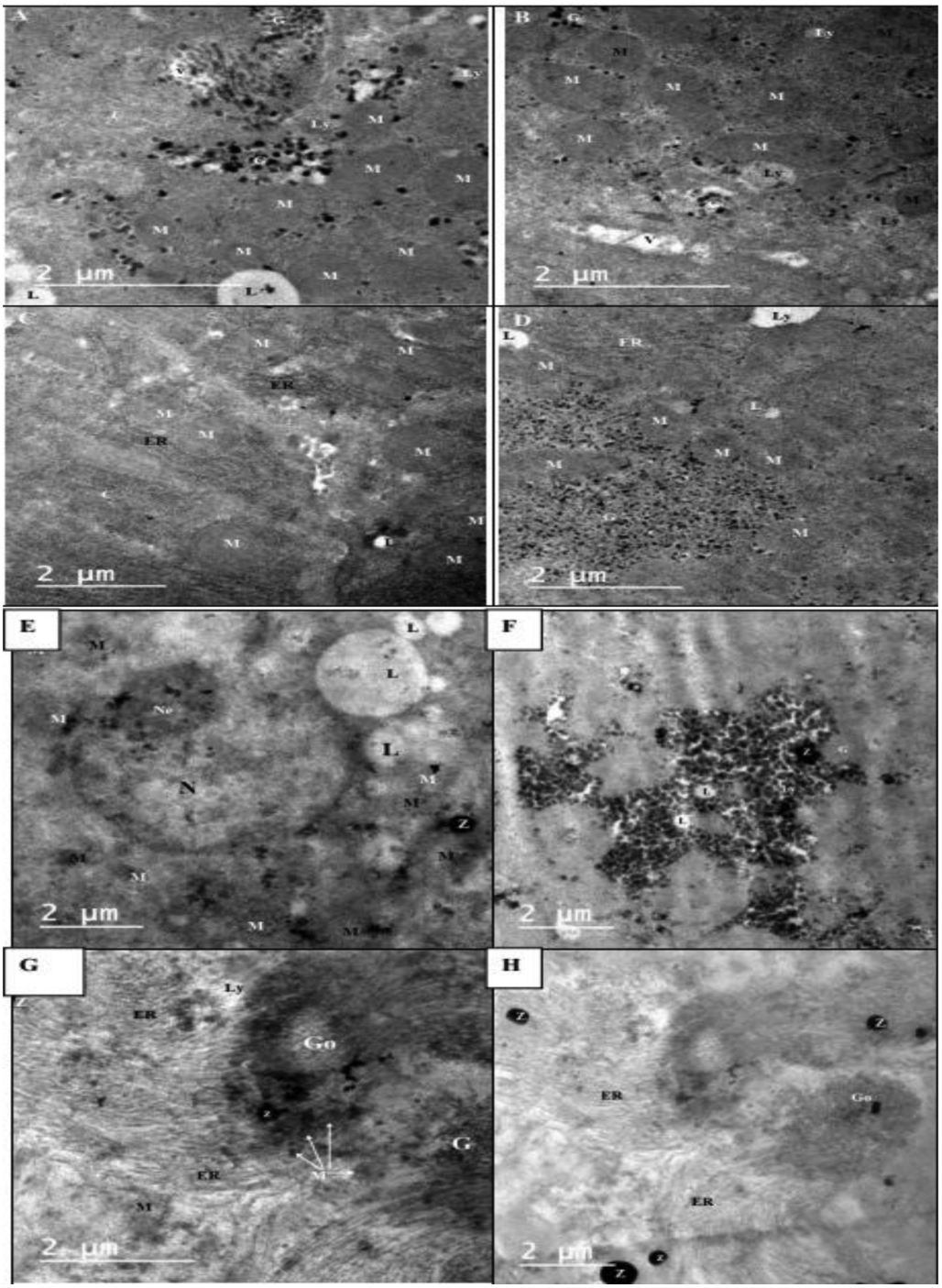

TEM of the rat liver treated with zinc nanoparticles (a–d) shows the nucleus (N), nucleolus (Ne), mitochondria (M), endoplasmic reticulum (ER) glycogen (G), lipid droplet (L), lysosomes (Ly), and zinc particles (z). The liver of rats treated with zinc nanoparticles and LPS (e–h) shows glycogen deposition (G), few mitochondria (M), endoplasmic reticulum (ER), lysosomes (Ly), and lipid (L), and Golgi apparatus (Go). LPS, lipopolysaccharide; TEM, transmission electron microscope.

veterinary fields as an alternative treatment of endometritis instead of the conventional antibiotic.

Acknowledgements

Authors' contributions: A.M.A. put forth the study design, made the statistical analysis, and wrote the manuscript. S.T.O. performed all the in vitro studies. M.A.S.A. performed the histopathological and electron microscope. M.S.K. performed the antioxidant analysis. A.H.A. performed the acute toxicity experiment and determined the LD50.

Financial support and sponsorship

Nil.

Table 2 Mean±SEM of malondialdehyde, nitric oxide, superoxide dismutase, and testosterone of rats treated with lipopolysaccharide, zinc oxide nanoparticles, and lipopolysaccharide+zinc oxide nanoparticles

Treatment	Control	LPS	Nano-zinc	Nano-zinc +LPS	*P* value
MDA (mol/ml)	17.16 ±1.15^{c}	13.99 ±.59^{b}	16.05 ±3.11^{c}	11.03 ±.68^{a}	0.0001
NO (mmol/l)	39.09 ±5.33^{c}	26.16 ±1.61^{a}	37.25 ±4.27^{bc}	33.59 ±1.02^{b}	0.0001
SOD (U/ml)	350 ±38^{a}	547 ±27^{b}	542 ±77^{b}	333±64^{a}	0.0001
Testosterone (ng/ml)	2.64 ±9.91^{b}	0.89 ±0.32^{a}	3.34 ±1.07^{b}	3.60 ±1.76^{b}	0.002

LPS, lipopolysaccharide; MDA, malondialdehyde; NO, nitric oxide; SOD, superoxide dismutase. Means with different superscripts (a, b, c) are significantly different at *P* value less than 0.05.

Conflicts of interest

There are no conflicts of interest.

References

1 Uçmak ZG, Kurban I, Uçmak M. Evaluation of vascularization in the walls of preovulatory follicles in mares with endometritis. Theriogenology 2020; 157:79–84.

2 Cui L, Wang H, Lin J, Wang Y, Dong J, Li J, *et al.* Progesterone inhibits inflammatory response in *E. coli*- or LPS-Stimulated bovine endometrial epithelial cells by NF-κB and MAPK pathways. Dev Comp Immunol 2020; 74:106508.

3 Miao Y, Ishfaq M, Liu Y, Wu Z, Wang J, Li R, *et al.* Baicalin attenuates endometritis in a rabbit model induced by infection with *Escherichia coli* and *Staphylococcus aureus* via NF-kB and JNK signaling Q1 pathways. Dom Anim Endocrinol 2020; 74:106508.

4 Jiang PY, Zhu XJ, Zhang YN, Zhou FF, Yang XF. Protective effects of apigenin on LPS-induced endometritis via activating Nrf2 signaling pathway. Microb Pathol 2018; 123:139–143.

5 O'Bryan MK, Schlatt S, Phillips DJ, de Kretser DM, Hedger MP. Bacterial lipopolysaccharide-induced inflammation compromises testicular function at multiple levels in vivo. Endocrinology 2000; 141:238–246.

6 Pelgrift RY, Friedman AJ. Nanotechnology as a therapeutic tool to combat microbial resistance. Adv Drug Deliv Rev 2013; 65:1803–1815.

7 da Silva BL, Abuçafy MP, Manaia EB, Oshiro Junior JA, Chiari-Andréo BG, Pietro RCIR, *et al.* Relationship between structure and antimicrobial activity of zinc oxide nanoparticles. An overview. Int J Nanomed 2019; 14;9395–9410.

8 Wang C, Lu J, Zhou L, Li J, Xu J, Li W, *et al.* Effects of long-term exposure to zinc oxide nanoparticles on development zinc metabolism and biodistribution of minerals (Zn Fe Cu Mn) in Mice. PLoS One 2016; 11: e0164434.

9 Yousef MI, Mutar TF, Kamel MAE. Hepato-renal toxicity of oral sub-chronic exposure to aluminum oxide and/or zinc oxide nanoparticles in rats. Toxicol Rep 2019; 6:336–346.

10 Khan FA, Akhtar S, Almofty SA, Almohazey D, Alomari M. FMSP-nanoparticles induced cell death on human breast adenocarcinoma cell line (MCF-7 Cells). Morphometr Anal Biomol 2018; 8:32.

11 Almansour M, Alarifi1 S, Melhim W, Jarrar BM. Nephron ultrastructural alterations induced by zinc oxide nanoparticles an electron microscopic study. IET Nanobiotechnol 2019; 13:59–65.

12 Pinho AR, Rebelo S, Pereira ML. The impact of zinc oxide nanoparticles on male infertility. Mater Basel 2020; 13:849.

13 Shen J, Yang D, Zhou X, Wang Y, Tang S, Yin H, *et al.* Role of autophagy in zinc oxide nanoparticles-induced apoptosis of mouse Leydig Cells. Int J Mol Sci 2019; 20:4042.

14 Han Z, Yan Q, Ge W, Liu Z-G., Gurunathan S, De Felici M, *et al.* Cytotoxic effects of ZnO nanoparticles on mouse testicular cells. Int J Nanomedicine 2016; 11:5187–5203.

15 Mohamed DA, Abdelrahman SA. The possible protective role of zinc oxide nanoparticles ZnONPs on testicular and epididymal structure and sperm parameters in nicotine-treated adult rats a histological and biochemical study. Cell Tissue Res 2019; 375:543–558.

16 Abdelnaby EA, Abo El-Maaty AM, Ragab RSA, Seida AA. Assessment of uterine vascular perfusion during the estrous cycle of mares in connection to circulating leptin and nitric oxide concentrations. J Equine Vet Sci 2016; 39:25–32.

17 Winn W, Allen S, Janda W, Koneman E, Procop G, Schreckenberger P. Koneman's Color Atlas and Textbook of Diagnostic Microbiology 6th ed. New York, USA: Lippincott Williams and Wilkins; 2006.

18 CLSI Performance Standards for Antimicrobial Disk Susceptibility Tests Twenty-Fourth Informational Supplement. National committee for clinical laboratory standards institute. Wayne, PA: USA; 2006.

19 Omara ST. MIC and MBC of honey and gold nanoparticles against methicillin-resistant MRSA and vancomycin-resistant VRSA coagulase-positive S aureus isolated from contagious bovine clinical mastitis. J Genet Eng Biotechnol 2017; 15:19–230.

20 Kong T, Zhang SH, Zhang JL, Hao XQ, Yang F, Zhang C, *et al.* Acute and cumulative effects of unmodified 50-nm Nano-ZnO on mice. Biol Trace Elem Res 2018; 185:124–134.

21 Medina J, Bolaños H, Mosquera-Sanchez LP, Rodriguez-Paez JE. Controlled synthesis of ZnO nanoparticles and evaluation of their toxicity in Mus musculus mice. Int Nano Lett 2018; 8:165–179.

22 Bancroft D, Stevens A, Turner R. Theory and practice of histological technique. 4th ed. Edinburgh, London, Melbourne: Churchill, Livingstone 2012.

23 Beehan DP, Wolfsdorf K, Elam J, Krekeler N, Paccamonti D, Lyle SK. The evaluation of biofilm-forming potential of *Escherichia coli* collected from the Equine female reproductive tract. J Equine Vet Sci 2015; 35:935–939.

24 Chipangura JK, Chetty T, Kgoete M, Naidoo V. Prevalence of antimicrobial resistance from bacterial culture and susceptibility records from horse samples in South Africa. Prev Vet Med 2017; 148:37–44.

25 Siddiqi KS, Rahman A, Husen TA. Properties of zinc oxide nanoparticles and their activity against microbes. Nanoscale Res Lett 2018; 13:141.

26 Dhandapani KV, Anbumani D, Gandhi AD, Annamalai P, Muthuvenkatachalam BS, Kavitha P. Green route for the synthesis of zinc oxide nanoparticles from Melia azedarach leaf extract and evaluation of their antioxidant and antibacterial activities. Biocatal Agric Biotechnol 2020; 24:101517.

27 Sohail MF, Rehman M, Hussain SZ, Huma Z, Shahnaz G, Khalid OSQ, *et al.* Green synthesis of zinc oxide nanoparticles by Neem extract as multi-facet therapeutic agents. J Drug Deliv Sci Technol 2020; 59:101911.

28 Obeizi Z, Benbouzid H, Ouchenane S, Yılmaz D, Culha M, Bououdina M. Biosynthesis of zinc oxide nanoparticles from essential oil of *Eucalyptus globulus* with antimicrobial and anti-biofilm activities. Mater Today Comm 2020; 25:101553.

29 Vishnupriya B, Nandhini GRE, Anbarasi G. Biosynthesis of zinc oxide nanoparticles using *Hylocereus undatus* fruit peel extract against clinical pathogens. Mate. Today; Proceedings. 2020.

30 Asamoah RB, Yaya A, Mensah B, Nbalayim P, Apalangya V, Bensah YD, *et al.* Synthesis and characterization of zinc and copper oxide nanoparticles and their antibacteria activity. Results Mater 2020; 7:100099.

31 Gao Y, Xu D, Ren D, Zeng K, Wu X. Green synthesis of zinc oxide nanoparticles using Citrus sinensis peel extract and application to strawberry preservation, a comparison study. LWT-Food Sci Technol 2020; 126:109297.

32 Mahendra C, Chandra MN, Murali M, Abhilash MR, Singh SB, Satish S, *et al.* Phyto-fabricated ZnO nanoparticles from *Canthium dicoccum* L, for antimicrobial, anti-tuberculosis and antioxidant activity. Process Biochemist 2020; 89:220–226.

33 Luo Z, Wu Q, Zhang M, Li P, Ding Y. Cooperative antimicrobial activity of CdTe quantum dots with rocephin and fluorescence monitoring for Escherichia coli. J Colloid Interface Sci 2011; 362:100–106.

34 Nair S, Sasidharan A, Rani VD, Menon D, Nair S, Manzoor K, *et al.* Role of size scale of ZnO nanoparticles and microparticles on toxicity toward bacteria and osteoblast cancer cells. J Mater Sci Mater Med 2009; 20:235.

35 Dimapilis EAS, Hsu CS, Mendoza RMO, Lu MC. Zinc oxide nanoparticles for water disinfection. Sustain Environ Res 2018; 28:47–56.

36 Shen Y, Liu B, Mao W, Gao R, Feng S, Qian Y, *et al.* PGE2 downregulates LPS-induced inflammatory responses via the TLR4-NF- κB signaling pathway in bovine endometrial epithelial cells prostaglandins. Leukot Essent Fatty Acids 2018; 129:25–31.

37 Babele PK, Thakre PK, Kumawat R, Tomar RS. Zinc oxide nanoparticles induce toxicity by affecting cell wall integrity pathway, mitochondrial

function and lipid homeostasis in Saccharomyces cerevisiae. Chemosphere 2018; 213:65–75.

38 Hu CW, Li M, Cui YB, Li DS, Chen J, Yang LY. Toxicological effects of TiO2 and ZnO nanoparticles in soil on earthworm *Eisenia fetida*. Soil Biol Biochem 2010; 42:586–591.

39 Peng X, Palma S, Fisher NS, Wong SS. Effect of morphology of ZnO nanostructures on their toxicity to marine algae. Aquat Toxicol Amsterdam Netherlands 2011; 102:186–196.

40 Bisht G, Rayamajhi S. ZnO nanoparticles: a promising anticancer agent. Nanobiomed (Rij) 2016; 3:9.

41 Chen P, Powell BA, Mortimer M, Ke PC. Adaptive interactions between zinc oxide nanoparticles and Chlorella species. Environ Sci Technol 2012; 46:12178–12185.

42 Sabry MM, Ahmed MM, Abdel Maksoud OM, Rashed L, Morcos MA, Abo El-Maaty AM, *et al.* Carnitine, apelin and resveratrol regulate mitochondrial quality control QC, related proteins and ameliorate acute kidney injury, role of hydrogen peroxide. Arch Physiol Biochemist 2020; 13:1–10.

43 Afifi M, Almaghrabi OA, Kadasa NM. Ameliorative effect of zinc oxide nanoparticles on antioxidants and sperm characteristics in streptozotocin-induced diabetic rat testes. Biomed Res Int 2015; 2015:153573.

44 Ansar S, Abudawood M, Alaraj ASA, Hamed SS. Hesperidin alleviates zinc oxide nanoparticle induced hepatotoxicity and oxidative stress. BMC Pharmacol Toxicol 2018; 19:65.

45 Bara N, Kaul G. Enhanced steroidogenic and altered antioxidant response by ZnO nanoparticles in mouse testis Leydig cells. Toxicol Ind Health 2018; 34:571–588.

46 Hussein MM, Ali HA, Saadeldin IM, Ahmed MM. Querectin alleviates zinc oxide nanoreprotoxicity in male albino rats. J Biochem Mol Toxicol 2016; 30:489–496.

47 Lao Y, Ouyang H, Huang X, Huang Y. Effect of bacterial endotoxin lipopolysaccharide treatment on duck Leydig cells. Anim Reprod 2019; 16:871–879.

48 Aitken RJ, Roman SD. Antioxidant systems and oxidative stress in the testes. Adv Exp Med Biol 2008; 636:154–171.

49 Halawa AA, ElAdl MA, Hamed MH, Balboula AZ, Elmetwally MA. Lipopolysaccharide prompts oxidative stress and apoptosis in rats' testicular tissue. J Vet Healthcare 2018; 1:20–31.

50 Metukuri MR, Reddy CM, Reddy PR, Reddanna P. Bacterial LPS mediated acute inflammation-induced spermatogenic failure in rats, role of stress response proteins and mitochondrial dysfunction. Inflammation 2010; 33:235–243.

51 Hassan A, Youssef MM, Khalil A, Ahmed H. Effects of bacterial lipopolysaccharide on serum testosterone level and sperm vitality in mature rats'. J Vet Med Res 2017; 24:163–168.

52 Li L, Ma P, Liu Y, Huang C, Wai-Sum O, Tang F, *et al.* Intermedin attenuates LPS-induced inflammation in the rat testis. PLoS One 2013; 8:e65278.

53 Doğanyiğit Z, Küp FÖ, Silici S, Deniz K, Yakan B, Atayoglu T. Protective effects of propolis on female rats' histopathological, biochemical and genotoxic changes during LPS induced endotoxemia. Phytomedicine 2013; 20:632–639.

54 Ranneh Y, Akim AM, Hamid HA, Khazaai H, Fadel A, Mahmoud AM. Stingless bee honey protects against lipopolysaccharide induced-chronic subclinical systemic inflammation and oxidative stress by modulating Nrf2, NF-κB and p38 MAPK. Nutr Metab 2019; 16:15.

55 Pandir D, Per S, Doğanyiğit Z, Bekdemir F, Gök G, Demirbağ A. All aspects of the toxic effects of lipopolysaccharide on rat liver and the protective effect of vitamin E and sodium selenite. Turk J Zool 2019; 43:566–579.

56 Forget P, Khalifa C, Defour JP, Latinne D, Van Pel MC, De Kock M. What is the normal value of the neutrophil-to-lymphocyte ratio? BMC Res Notes 2017; 10:1–4.

57 Hosseini SM, Moshrefi HA, Amani R, Razavimehr SV, Aghajanikhah MH, Sokouti Z, *et al.* Subchronic effects of different doses of Zinc oxide nanoparticle on reproductive organs of female rats, an experimental study. Int J Reprod Biomed 2018; 17:107–118.>.